Improving Efficacy and Safety of Agonistic Anti-CD40 Antibody Through Extracellular Matrix Affinity

Authors: Jun Ishihara[1]*, Ako Ishihara[1]*, Lambert Potin[1,2], Peyman Hosseinchi[1], Kazuto Fukunaga[1,+], Martina Damo[1,++], Thomas F. Gajewski[3,4], Melody A. Swartz[1,4], and Jeffrey A. Hubbell[1]

Authors' Affiliations:

1 Institute for Molecular Engineering, University of Chicago, Chicago, IL 60637, USA.

2 Institute of Bioengineering, Ecole Polytechnique Fédérale de Lausanne, CH-1015 Lausanne, Switzerland.

3 Department of Pathology, University of Chicago, Chicago, IL 60637, USA.

4 Ben May Department of Cancer Research, University of Chicago, Chicago, IL 60637, USA.

*These authors contributed equally.

[+] Current address: Department of Bioengineering, Tokyo Institute of Technology, 226-8501 Yokohama, Kanagawa, Japan.

[++] Current address: Yale School of Medicine, New Haven, CT 06510, USA.

Corresponding Author: Jeffrey A. Hubbell, 5640 S. Ellis Avenue, Chicago, IL 60637, USA. Phone: +1 773-702-0585 E-mail: jhubbell@uchicago.edu

Running Title:

ECM-binding character improves anti-CD40 antibody.

Key Words:

Cancer immunotherapy, antigen-presenting cells, T cell activation, tumor inflammation, drug delivery

One Sentence Summary:

Extracellular matrix-binding peptide conjugation to agonistic anti-CD40 antibody enhances antitumor efficacy and reduces treatment-related adverse events.

Grant Support This work was funded in part by the European Research Commission

grant Cytrix to J.A. Hubbell. L. Potin was funded by the Fonds Pierre-François Vittone.

Disclosure of Potential Conflicts of Interest J. Ishihara, A. Ishihara, K. Fukunaga, M.A. Swartz and J.A. Hubbell are inventors on US provisional patent application 62/487,823 that covers the matrix-binding antibody technology presented in this report.

Abstract

CD40 is an immune co-stimulatory receptor expressed by antigen-presenting cells. Agonistic anti-CD40 antibodies have demonstrated considerable anti-tumor effects yet can also elicit serious treatment-related adverse events, such as liver toxicity, including in man. We engineered a variant that binds extracellular matrix through a super-affinity peptide derived from placenta growth factor-2 (PlGF-$2_{123-144}$) to enhance anti-CD40's effects when administered locally. Peri-tumoral injection of PlGF-$2_{123-144}$-anti-CD40 antibody showed prolonged tissue retention at the injection site and substantially decreased systemic exposure, resulting in decreased liver toxicity. In four mouse tumor models, PlGF-$2_{123-144}$-anti-CD40 antibody demonstrated enhanced antitumor efficacy compared to its unmodified form and correlated with activated dendritic cells, B cells,

and T cells in the tumor and in the tumor-draining lymph node. Moreover, in a genetically engineered $Braf^{V600E}$ βCat^{STA} melanoma model that does not respond to checkpoint inhibitors, PlGF-$2_{123-144}$-anti-CD40 antibody treatment enhanced T cell infiltration into the tumors and slowed tumor growth. Together, these results demonstrate the marked therapeutic advantages of engineering matrix binding domains onto agonistic anti-CD40 antibody as a therapeutic given by tumoriregional injection for cancer immunotherapy.

Introduction

CD40 (tumor necrosis factor receptor superfamily 5: TNFRSF5) is a 48 kDa type I transmembrane protein expressed by antigen-presenting cells (APCs) (1). CD40 mediates an activation signal on APCs when ligated by CD40L (CD154), expressed predominantly by activated helper T cells.

Agonistic antibodies against CD40 (αCD40) have been shown to suppress tumor growth in both mouse models and clinical trials (2-11). On DCs, αCD40 increases cell-surface expression of co-stimulatory and major histocompatibility

complex (MHC) molecules and induces pro-inflammatory cytokines, leading to enhanced B and T cell activation (2,12-14). αCD40 binding on follicular B cells induces proliferation, immunoglobulin class switching, and secretion of antitumor antibodies (4,15). B cell depletion partially impairs the antitumor efficacy of αCD40 treatment in murine malignant mesothelioma (4). On tumor-associated macrophages, αCD40 treatment drives phenotype switching from M2 to M1 type, which is accompanied by induction of cytotoxic T cell and natural killer (NK) cell responses against tumors (6,7). Thus, αCD40 treatment can induce anti-tumor effects through activation of several cell types, both directly (APCs, including B cells) and indirectly (T cells, NK cells).

Several agonistic αCD40 antibodies have been developed for human cancer immunotherapy (e.g. CP-870,893, dacetuzumumab, ADC-1013, and Chi Lob 7/4) and have shown favorable antitumor responses in melanoma, pancreatic carcinoma, mesothelioma, and lymphoma (1,8,9). However, much remains to be improved with αCD40 therapy; for example, treatment-related adverse events such as interleukin-6 (IL-6) and tumor necrosis factor-α (TNF-α) cytokine release syndrome and hepatotoxicity have been reported after αCD40 treatment in the clinic (11), limiting the

dosage of αCD40 treatment (1). To address these issues, local injection of αCD40 such as intra-tumoral or peri-tumoral (p.t.) injection has been tested and has shown higher antitumor efficacy compared to systemic injection (e.g. intra-venous or intra-peritoneal injection) in several mouse tumor models (2,16-18). Based on these results, intra-tumoral injection of αCD40 (ADC-1013) is now being explored in a clinician trial (19).

Immune checkpoint inhibitor (CPI) therapy such as cytotoxic T-lymphocyte-associated protein 4/programmed cell death 1 (CTLA4/PD-1) inhibition exhibits considerable antitumor activity in the clinic (20-22). Because the main mechanism of CTLA4/PD-1 inhibition therapy is antitumor T cell activation, the success of CPI therapy is largely dependent on T cell infiltration into the tumor (23,24). However, partially due to poor T cell infiltration, a substantial number of patients do not respond to CPI therapy. The response rates against advanced melanoma for monotherapies range from 19% for αCTLA4 (ipilimumab) to 44% for αPD-1 (nivolumab) (25). Therefore, the development of alternative strategies as mono- or adjunctive therapies to enhance T cell infiltration into tumors is needed for tumor immunotherapy.

We have previously discovered that the heparin-binding domain of placenta growth factor-2 (PlGF-$2_{123-144}$) binds to multiple extracellular matrix (ECM) proteins with particularly high affinity of 1-10 nM dissociation constant (K_d) values (26), and we have developed PlGF-$2_{123-144}$ peptide-conjugated CPI antibodies (αCTLA4 and anti-programmed cell death ligand 1 (αPD-L1)) to enhance tissue retention at the local injection site and decrease systemic antibody levels (27). This led to a marked reduction in treatment-related adverse events, such as hepatotoxicity and autoimmune diabetes development in mouse models. The combination treatment of PlGF-$2_{123-144}$-αCTLA4 and PlGF-$2_{123-144}$-αPD-L1 showed markedly higher antitumor efficacy compared to their unmodified forms in mouse models of melanoma and breast cancer.

Here, we hypothesized that αCD40 could also be rendered more effective and safer in cancer immunotherapy by modification with the ECM-binding property derived from PlGF-$2_{123-144}$ peptide conjugation. Our objective was to develop an approach to improve the antitumor effects of agonistic αCD40 immunotherapy against both CPI-responsive and CPI-unresponsive tumors, while reducing the treatment-related adverse events through lowering systemic exposure to αCD40.

Materials and methods

Synthesis of PlGF-$2_{123-144}$-αCD40

The synthesis of PlGF-$2_{123-144}$-αCD40 was performed as described previously for PlGF-$2_{123-144}$-αCTLA4 and PlGF-$2_{123-144}$-αPD-L1 (27). Rat anti-mouse CD40 (clone: FGK4.5, BioXCell) was incubated with 15 eq. of sulfo-succinimidyl 4-(N-maleimidomethyl) cyclohexane-1-carboxylate (sulfo-SMCC) for 30 min at room temperature. Excess sulfo-SMCC was removed using a Zeba spin desalting column (Thermo Fisher Scientific). 15 eq. of PlGF-$2_{123-144}$ peptide (RRRPKGRGKRRREKQRPTDCHL) was then added and reacted for 1 hr at room temperature for conjugation to the thiol moiety on the C residue. The peptide had been synthesized with > 95% purity by Genscript.

Sodium dodecyl sulfate polyacrylamide gel electrophoresis (SDS-PAGE)

Characterization of peptide conjugation to αCD40 was performed as described previously for PlGF-$2_{123-144}$-rat IgG2a, for example (27). SDS-PAGE was performed on

4-20% gradient gels (Bio-Rad) after αCD40 was reduced with 10 mM DTT. After electrophoresis, gels were stained with SimplyBlue SafeStain (Thermo Fisher Scientific) according to the manufacturer's instruction. Gel images were acquired with the ChemiDoc XRS+ system (Bio-Rad).

Binding assay

Characterization of ECM protein affinity of PlGF-$2_{123-144}$-αCD40 was performed as described previously for PlGF-$2_{123-144}$-αCTLA4, for example (27). 96-well ELISA plates (Greiner Bio One) were coated with 10 μg/mL recombinant human ECM proteins, fibronectin (Sigma-Aldrich), vitronectin (Sigma-Aldrich), collagen I (EMD Millipore), or with 1 μg/mL recombinant mouse (rm) CD40 (Sino Biological) in phosphate-buffered saline (PBS) for 1 hr at 37°C, followed by blocking with 2% bovine serum albumin (BSA) in PBS with 0.05% Tween 20 (PBS-T) for 1 hr at room temperature. Then, wells were washed with PBS-T and further incubated with PlGF-$2_{123-144}$- or unmodified αCD40 (10 μg/mL for ECM proteins) for 1 hr at room temperature. After 3 washes with PBS-T, wells were incubated for 1 hr at room

temperature with horseradish peroxidase (HRP)-conjugated antibody against rat IgG (Jackson ImmunoResearch). After washes, bound αCD40 was detected with tetramethylbenzidine substrate by measurement of the absorbance at 450 nm with subtraction of the signal at 570 nm.

Dendritic cell stimulation

Bone marrow cells from C57BL/6 mouse (Jackson Laboratories) tibiae and femurs were expanded for 9 d with 20 ng/mL GM-CSF (Peprotech), with fresh medium and cytokines added at day 3 and 6. On day 9, cells were washed and resuspended on non-tissue culture-treated 96-well U-bottom plates, at 10^5 cells/200 µL. The bone marrow-derived DCs (BMDCs) were stimulated overnight in the presence of 1 µg/mL (or equimolar concentrations) of rat IgG2a (BioLegend), αCD40, or αCD40 crosslinked using rabbit anti-rat IgG (Fc specific, Sigma-Aldrich). The crosslinking agent was mixed for 40 min at room temperature at a 2:1 molar ratio before being added to the culture media. Cells were harvested for flow cytometric analysis. For immunostaining, CD11c (HL3, BD Biosciences), CD80 (16-10A1, BD Biosciences), CD86 (GL-1, BD

Biosciences), MHCII (M5/114.15.2, BioLegend) were used. DCs were gated as $CD11c^{+}MHCII^{+}$.

Mice and cell lines

Athymic nude (for imaging), C57BL/6 (for B16F10 melanoma model), Balb/c (for CT26 colon carcinoma model) and FVB (for MMTV-PyMT breast cancer model) mice, age 8-12 wk, were obtained from the Jackson Laboratories. *Batf3*$^{-/-}$ mice, age 8-12 wk, were a kind gift from Dr. Justin Kline (University of Chicago). *Tyr:Cre-ER*$^{+}$*/LSL-Braf*^{V600E}*/Pten*$^{fl/fl}$ *βCat*^{STA} mice, age 6-12 wk, were generated as reported previously and bred at the animal facility of the University of Chicago according to the institutional guidance (28). Experiments were performed with approval from the Institutional Animal Care and Use Committee of the University of Chicago (protocol number 72470). B16F10 cells and CT26 cells were obtained from the American Type Culture Collection and cultured according to the instructions. MMTV-PyMT cells were obtained from spontaneously developed breast cancer in FVB-Tg (MMTV-PyVT) transgenic mice (polyoma middle T antigen oncogene

expression was induced by mouse mammary tumor virus promotor) and cultured *in vitro*. All cell lines used in this study were checked for mycoplasma contamination by IMPACT I pathogen test (IDEXX BioResearch).

αCD40 skin retention analysis

αCD40 was fluorescently labeled using sulfo-Cyanine 7 NHS ester (Lumiprobe) according to the manufacture's instruction. PlGF-$2_{123-144}$ peptide that is labeled with Cyanine 7 in its N-terminus was chemically synthesized with >90 % purity by Thermo Fisher Scientific. Cyanine 7-labeled PlGF-$2_{123-144}$ was conjugated to αCD40 as described above. Athymic nude mice were injected with 40 μg of PlGF-$2_{123-144}$- or unmodified Cyanine 7 labeled αCD40 intra-dermally (i.d.). Mice were imaged every 24 hr after injection with a Xenogen IVIS Imaging System 100 (Xenogen) under the following conditions: f/stop: 2; optical filter excitation 710 nm; excitation 780 nm; exposure time: 1 sec; small binning.

Antibody concentration analysis

Measurement of antibody concentration in circulation was performed as described previously (27). 5×10^5 B16F10 melanoma cells were injected intradermally on the left side of the back of each 12 wk old C57BL/6 mouse. After 4 days, mice were injected with 50 μg of αCD40 peri-tumorally (p.t.). Blood samples were collected in tubes on days 4 (4 hr after αCD40 injection on this post-inoculation day), 6, and 8 days after tumor inoculation. Concentrations of αCD40 in serum were measured by ELISA as described above.

Serum cytokine concentration analysis

Serum cytokine concentrations were measured as described previously (27). 5×10^5 B16F10 melanoma cells were injected intradermally on the left side of the back of each 12 wk old C57BL/6 mouse. After 4 days, mice received two doses of 50 μg αCD40. On day 4 (4 hr after αCD40 injection), 5, 6, and 8, blood samples were collected in tubes, followed by overnight incubation at 4°C. Cytokine concentrations in serum were measured by Ready-SET-Go! ELISA kits (eBioscience) according to the manufacturer's protocol.

ALT activity analysis

Serum alanine aminotransferase (ALT) activity was measured as described previously (27). B16F10 tumor bearing mice received 50 μg αCD40 injection, 4 days after tumor inoculation. On day 5, 7, and 9, blood samples were collected in tubes, followed by > 4 hr incubation at 4°C. ALT activity in serum was measured by ALT assay kit (Sigma-Aldrich) according to the manufacturer's protocol.

Histology

Liver histology was performed as described previously (27). B16F10 tumor-bearing mice received 50 μg αCD40 injection, 4 days after tumor inoculation. 7 days after tumor inoculation, livers were collected and fixed with 2% paraformaldehyde. After embedding in paraffin, blocks were cut into 5 μm sections, followed by staining with hematoxylin and eosin. Images were captured with an EVOS FL Auto microscope (Life Technologies).

RNA extraction and gene expression analysis of CD40

Lymph node (LN) cells and hepatocytes were freshly isolated from C57BL/6 mice as previously described (29,30). Total RNA was extracted from LN cells and hepatocytes using the RNeasy micro kit isolation protocol (Qiagen) according to manufacturer's instructions. cDNA was obtained by reverse transcription polymerase chain reaction (RT-PCR) of total RNA performed using the SuperScript III First Strand Synthesis SuperMix (Life Technologies) following manufacturer's instructions. Gene expression analysis was performed by TaqMan gene expression assays specific for *CD40* (Mm00441891_m1) and *β-Actin* (Mm01268569_m1) (Life Technologies) in a LightCycler 96 System (Roche). Relative gene expression was quantified using the formula (gene expression fold change) = $2^{(\text{Cq } \textit{Actin} - \text{Cq } \textit{CD40})}$ with *β-Actin* as reference gene.

Antitumor efficacy of αCD40 on B16F10 melanoma

Antitumor efficacy in the B16F10 melanoma model was performed as described previously (27). A total of 5×10^5 B16F10 cells re-suspended in 50 μL of PBS were

inoculated intradermally on the left side of the back of each C57BL/6 mouse or *Batf3*$^{-/-}$ mouse. After 4 days, mice were injected with 10 μg or 50 μg of αCD40 p.t. For distant tumor experiments, 5×10^5 B16F10 cells were injected intradermally on the left and right sides of the back of each mouse on day 0. On day 4, mice were injected with 50 μg of αCD40 p.t. beside only the left tumor. For combination therapy with CPI, 100 μg each of rat anti-mouse PD-L1 (clone: 10F.9G2, Bio X Cell) and hamster anti-mouse CTLA4 (clone: 9H10, Bio X Cell) antibodies were used. Tumors were measured with a digital caliper starting 4 days after first tumor inoculation, and volumes were calculated as ellipsoids, where V = 4/3 × 3.14 × depth/2 × width/2 × height/2. Mice were sacrificed at the point when either tumor volume had reached over 500 mm^3.

Antitumor efficacy of αCD40 on CT26 colon carcinoma

A total of 5×10^5 CT26 colon carcinoma cells re-suspended in 50 μL of PBS were inoculated intradermally on the left side of the back of each Balb/c mouse. After 5 days, mice were injected with 10 μg of αCD40 intradermally p.t. Tumors were measured with

a digital caliper starting 5 days after tumor inoculation as described above. Mice were sacrificed at the point when either tumor volume had reached over 500 mm^3.

Antitumor efficacy of αCD40 on MMTV-PyMT breast cancer

Antitumor efficacy in the MMTV-PyMT breast cancer model was performed as described previously (27). A total of 8×10^5 MMTV-PyMT cells re-suspended in 50 μL of PBS were injected subcutaneously into the mammary fat pad on the right side of each FVB mouse. After 7 days, mice were injected with 50 μg of αCD40 p.t. Tumors were measured with a digital caliper as described above. Mice were sacrificed when tumor volume reached over 500 mm^3.

Tissue and cell preparation and T cell subset analysis

T cell phenotyping in tumor, spleen and LN tissue was performed as described previously (27). 5×10^5 B16F10 melanoma cells were injected intradermally on the left side of the back of each C57BL/6 mouse. After 4 and 7 days, mice were injected with 50 μg of αCD40 p.t.. Mice were sacrificed on day 8. Spleens, LNs, and

tumors were harvested. Tumors were digested in Dulbecco's Modified Eagle Medium (DMEM) supplemented with 2% FBS, 2 mg/mL collagenase D and 40 μg/mL DNase I (Roche) for 30 min at 37°C. Single-cell suspensions were obtained by gently disrupting the tissues through a 70-mm cell strainer. Red blood cells were lysed with ACK lysing buffer (Quality Biological). Cells were counted and re-suspended in Iscove's Modified Dulbecco's Medium (IMDM) supplemented with 10% FBS and 1% penicillin/streptomycin (full medium; all from Life Technologies) and used for flow cytometry staining.

Flow cytometry and antibodies

Flow cytometry was performed as described previously (27). Single cell suspensions from spleens, td-LNs, and tumors were prepared as described above. Following a washing step, approximately 2×10^6 cells were used for antibody staining. Antibodies were purchased from BD Biosciences if not otherwise indicated: CD3 (145-2C11), CD4 (RM4-5), CD8α (53–6.7), CD11c (HL3), CD25 (M-A251), CD44 (IM7), CD45 (30-F11), CD62L (MEL-14), CD86 (GL-1), F4/80 (T45-2342), Foxp3

(MF23), NK1.1 (PK136), MHCII (M5/114.15.2, BioLegend), PD-1 (29F.1A12, BioLegend). Fixable live/dead cell discrimination was performed using Fixable Viability Dye eFluor 455 (eBioscience) according to the manufacturer's instructions. Staining was carried out on ice for 20 min if not indicated otherwise, and intracellular staining was performed using the Foxp3-staining kit according to manufacturer's instructions (BioLegend). Following a washing step, cells were stained with specific antibodies for 20 min on ice prior to fixation. All flow cytometric analyses were done using a Fortessa (BD Biosciences) flow cytometer and analyzed using FlowJo software (FlowJo, LLC.).

Endogenous antibody detection

B16F10 tumor bearing mice received 10 μg αCD40 injection, 4 days after tumor inoculation. On day 11, blood plasma samples were collected in heparinized tubes. B16F10 cells were incubated with 10% plasma in PBS from treated mice (day 11) for 60 min at 4°C, washed twice with PBS, and then incubated with Alexa-Fluor-647-labeled rat anti-mouse-IgG (Jackson Immunoresearch) for 30 min at 4 °C.

After cells were washed in PBS, the mean fluorescence intensity was analyzed using a Fortessa cytometer.

Tyr:Cre-ER^{+}/LSL-Braf^{V600E}/Pten$^{fl/fl}$ βCat^{STA} melanoma induction and antibody injection

6-12 wk-old _Tyr:Cre-ER^{+}/LSL-Braf^{V600E}/Pten$^{fl/fl}$ βCat^{STA}_ mice were shaved on the back and 5 µL of 4-OH-tamoxifen (Sigma-Aldrich) at 10 mg/mL was applied topically, as previously described (28). Right after the visible tumor development (day 0) and again on day 7, mice were injected with 10 µg of αCD40 p.t. Volume was calculated as Volume = Surface * Z, where Surface is computed through ImageJ analysis and Z is the thickness of the tumor, measured with a digital caliper. Mice were sacrificed at the point when tumor volume had reached over 1000 mm^3.

Analysis of tumor-infiltrating T cell density

After euthanasia of a tumor-bearing mouse, part of the tumor was fixed with zinc fixative. Histological analysis was performed on serial sections (7 µm frozen

sections) from the central portion of the melanoma. Cryosections blocked with 2% BSA in tris-buffered saline with TBS-T, were incubated with hamster anti-mouse anti-CD31 antibody (2H8, Abcam), rabbit anti-mouse anti-CD3 antibody (SP7, Abcam) and rat anti-mouse anti-CD8 antibody (53-6.7, BioLegend). After washing with TBS-T, sections were incubated with Alexa Fluor 488-conjugated anti-hamster antibody, Alexa Fluor 594-conjugated anti-rabbit antibody or Alexa Fluor 647-conjugated anti-rat antibody (Jackson ImmunoResearch) for 1 hr at room temperature. Images were taken with IX83 microscope (Olympus). After images were taken, the number of tumor-infiltrating $CD8^+$ T cells was counted using ImageJ software. Tumor-infiltrating $CD8^+$ T cells were defined as double-positive (co-localization) for CD8 and CD3, excluding the cells that are within the $CD31^+$ vessels. Intra-tumoral area was identified and calculated using bright field images.

Statistical analysis

Multiple batches of PlGF-$2_{123\text{-}144}$-αCD40 were synthesized by multiple individuals, and tumor treatments were performed by multiple individuals to ensure reproducibility. For

animal studies, mice were randomized into treatment groups within a cage immediately before the first αCD40 injection and treated in the same way. Statistically significant differences between experimental groups were determined using Prism software (v7, GraphPad). Statistical analyses were done using one-way ANOVA followed by Tukey's HSD post hoc test. For single comparisons, a two-tailed Student's *t*-test was used. Survival curves were analyzed by using the log-rank (Mantel–Cox) test. All experiments are replicated at least twice. The symbols * and ** indicate P values less than 0.05 and 0.01, respectively; N.S., not significant.

Results

PlGF-$2_{123-144}$ peptide conjugation enhances ECM binding and prolongs tissue retention of αCD40

We first characterized and validated the ECM-binding properties of PlGF-$2_{123-144}$-αCD40 *in vitro*. SDS-PAGE revealed that the molecular weights of both the light and heavy chains of αCD40 were increased. Indeed, we have previously reported that around 6 PlGF-$2_{123-144}$ peptides are crosslinked to 1 IgG under these

reaction conditions (Fig. 1A) (27). PlGF-$2_{123-144}$-αCD40 was shown to bind to fibronectin, vitronectin, and collagen I, tested as major ECM proteins (Fig. 1B). In comparison, unmodified αCD40 did not bind to the tested ECM proteins. PlGF-$2_{123-144}$-αCD40 recognized recombinant mouse CD40 with a similar K_d value as the unmodified antibody (Fig. 1C). These data show that PlGF-$2_{123-144}$-modification of αCD40 led to strong ECM binding without impairing its antigen recognition. It has been reported that engagement of Fc-receptor by αCD40 (specifically, Fc-crosslinking to αCD40) is required for optimal activation of APCs (31). Interestingly, PlGF-$2_{123-144}$ conjugation had greater activation of DCs compared to its unmodified form, even when it was not crosslinked, suggesting that PlGF-$2_{123-144}$ conjugation improves APC activation by acting to positively influence Fc crosslinking as well (Supplemental fig. S1).

Next, we examined the tissue retention capacity of PlGF-$2_{123-144}$-αCD40. Using *in vivo* imaging analysis, we could still detect that PlGF-$2_{123-144}$-αCD40 was retained at the injection site long-term through binding to endogenous ECM molecules. The signal of PlGF-$2_{123-144}$-αCD40 was detectable at the injection site for 96 hr after

injection, whereas the signal of unmodified αCD40 became very low after 48 hr from injection. This data shows that PlGF-$2_{123-144}$ conjugation enhanced retention of αCD40 at the tissue injection site (Fig. 1D).

PlGF-$2_{123-144}$ conjugation lowers αCD40 systemic exposure and prevents treatment-related adverse events

Because PlGF-$2_{123-144}$-αCD40 showed prolonged retention at the injection site, we hypothesized that the concentration of the injected PlGF-$2_{123-144}$-αCD40 in blood serum would be lower compared to unmodified αCD40, due to retention in the tumor injection site. We measured αCD40 concentrations in blood serum over time after a single peri-tumoral (p.t.) administration (50 μg) of αCD40 in B16F10 tumors 4 d after inoculation. The concentration of PlGF-$2_{123-144}$-αCD40 in blood serum was lower compared to αCD40 at all time points. This lower systemic exposure suggests that PlGF-$2_{123-144}$ conjugation might decrease systemic toxicity of αCD40.

Next, treatment-related adverse events were examined. αCD40 was injected p.t. 4 days after B16F10 tumor inoculation, then blood serum was collected.

Unmodified αCD40 administration significantly increased both IL-6 and TNFα concentrations in serum, whereas PlGF-$2_{123-144}$-αCD40 did not (Fig. 2B-C). Hepatotoxicity was investigated by measuring a clinically used liver damage marker, ALT activity. Unmodified αCD40 increased ALT activity levels compared to the PBS-treated group, but PlGF-$2_{123-144}$-αCD40 did not (Fig. 2D). In addition, histologic analysis of the liver showed that αCD40 induced marked morphological changes, as evidenced by hepatic necrosis and leukocyte infiltration (Fig. 2E). In contrast, no necrotic regions were observed after PlGF-$2_{123-144}$-αCD40 treatment, although some perivascular lymphocytic infiltration was still observed. mRNA of CD40 was not detected in hepatocytes (Supplemental fig. S2), consistent with an immunological rather than direct mechanism of hepatotoxicity (32). Taken together, these results indicate that PlGF-$2_{123-144}$ conjugation reduces the systemic toxicity of αCD40, likely through reduction of systemic exposure.

PlGF-$2_{123-144}$-αCD40 showed higher antitumor efficacy in multiple tumor models compared to unmodified αCD40

αCD40 administration has been tested at different doses in the clinic (9,12,16,33). Thus, we tested the antitumor efficacy of PlGF-$2_{123-144}$-αCD40 treatment at different doses in multiple mouse models that demonstrate T cell infiltration and thus are to an extent responsive to CPI. Four days after B16F10 cell inoculation, αCD40 (10 or 50 μg/injection) was administered p.t. At the dose of 10 μg/injection, PlGF-$2_{123-144}$-αCD40 treatment statistically significantly slowed tumor growth, whereas unmodified αCD40 did not show an antitumor effect (Fig. 3A). With an increased dose (50 μg/injection), unmodified αCD40 significantly slowed tumor growth and PlGF-$2_{123-144}$-αCD40 induced an even smaller tumor size, significantly more so than the unmodified antibody (Fig. 3B). Next, we investigated antitumor efficacy against CT26 colon carcinoma (Fig. 3C). Five days after CT26 cells were inoculated, αCD40 was administered at 10 μg/injection p.t.. PlGF-$2_{123-144}$-αCD40 treatment statistically significantly slowed tumor growth, whereas unmodified αCD40 did not show an antitumor effect (Fig. 3C). Similarly, we examined the antitumor activity of PlGF-$2_{123-144}$-αCD40 in the MMTV-PyMT genetically engineered breast cancer model (34) and found that p.t. administration of PlGF-$2_{123-144}$-αCD40 (50 μg/injection) again

suppressed tumor growth significantly stronger than its unmodified form (Fig. 3D). PlGF-$2_{123-144}$-αCD40 administration induced eradication of tumors in 2 out of 9 mice; unmodified αCD40 treatment eradicated tumors in 1 of 8 mice. These data indicated that local treatment with PlGF-$2_{123-144}$-αCD40 exhibits superior antitumor efficacy compared to local treatment with its unmodified form in multiple tumor types.

PlGF-$2_{123-144}$-αCD40 treatment effectively activates T cells, B cells, and DCs within the tumor and td-LN

To investigate the mechanisms behind the therapeutic action of PlGF-$2_{123-144}$-αCD40 treatment, T cell and APC responses were analyzed in B16F10 tumor-bearing mice. 50 μg αCD40 was injected p.t. on day 4 after tumor inoculation. On day 9, leukocytes were extracted from the tumor and td-LN. The frequency of DCs as a percentage of $CD45^+$ cells within the tumor was slightly decreased by unmodified αCD40 treatment (Fig. 4A). Both PlGF-$2_{123-144}$-αCD40 and unmodified αCD40 significantly increased the frequency of $CD11c^+$ DCs in the td-LN (Fig. 4B). Both PlGF-$2_{123-144}$-αCD40 and unmodified αCD40 treatments significantly decreased the

frequency of $MHCII^{High}CD86^{+}$ of $CD11c^{+}$ DCs in the tumor while increasing them in td-LN, indicating the maturation of $CD11c^{+}$ DCs (Fig. 4C). Similarly, the frequency of $MHCII^{High}CD86^{+}$ within $F4/80^{+}$ macrophages was significantly decreased in the tumor while being significantly increased in td-LN by both PlGF-$2_{123-144}$-αCD40 and unmodified αCD40 treatments, suggesting that αCD40 treatments induced activation of macrophages (Fig. 4E-F).

Regarding T cells, PlGF-$2_{123-144}$-αCD40 treatment significantly increased the frequency of $CD8^{+}CD3^{+}$ T cells of $CD45^{+}$ cells within the tumor compared to the PBS-treated group, while unmodified αCD40 treatment did not (Fig. 4G). PlGF-$2_{123-144}$-αCD40 treatment significantly increased the frequency of the effector population (defined as $CD62L^{-}CD44^{+}$) of $CD8^{+}CD3^{+}$ T cells within the tumor compared to the PBS-treated and unmodified αCD40-treated groups, indicating higher activation of $CD8^{+}$ T cells (Fig. 4H). Neither unmodified- nor PlGF-$2_{123-144}$-conjugated αCD40 treatments altered the frequency of $CD4^{+}CD3^{+}$ T cells of $CD45^{+}$ cells (Fig. 4I). The frequency of $CD25^{+}Foxp3^{+}$ Treg population of $CD4^{+}CD3^{+}$ T cells within the tumor was maintained in all treatment groups (Fig. 4J). Therefore, PlGF-$2_{123-144}$-αCD40 treatment

significantly increased the ratio of effector $CD8^+$ T cell/ Treg cell numbers within the tumor compared to PBS and unmodified αCD40 treatment groups (Fig. 4K). Unmodified αCD40 treatment slightly decreased the frequency of PD-1^+ of $CD8^+CD3^+$ T cells within the tumor compared to the PBS-treated group (Fig. 4L), consistent with previous research showing that αCD40 treatment reverses PD-1^+ exhausted tumor-infiltrated T cells into active cells (35).

In terms of B cell activation, we analyzed the tumor and blood on day 11. The frequency of $MHCII^{High}CD86^+$ within B cells was significantly enhanced by PlGF-$2_{123-144}$-αCD40 both in the tumor and td-LN, whereas αCD40 treatment increased the frequency of $MHCII^{High}CD86^+$ within B cells only in the td-LN (Fig. 4M-N). This data suggests that PlGF-$2_{123-144}$-αCD40 treatment induced activation of B cells. Crucially, PlGF-$2_{123-144}$-αCD40 treatment, but not unmodified αCD40 treatment, significantly increased induction of endogenous cell surface-binding antibodies against B16F10 cells (Fig. 4O), suggesting the B cell mediated antitumor mechanism as well.

The frequency of NK cells was maintained between all treatment groups within the tumor (Supplemental fig. S3A). Unmodified αCD40 treatment slightly

increased the frequency of NK cells in td-LN (Supplemental fig. S3B).

Collectively, PlGF-$2_{123\text{-}144}$-αCD40 treatment effectively activated T cells, DCs, B cells, and macrophages in the tumor or td-LN, consistent with the increased therapeutic effects reported in Fig. 3.

PlGF-$2_{123\text{-}144}$-αCD40 treatment induces systemic antitumor immunity through $CD8^+$ T cell priming

The increase of mature APCs and activated $CD8^+$ T cells after PlGF-$2_{123\text{-}144}$-αCD40 treatment led us to investigate whether PlGF-$2_{123\text{-}144}$-αCD40 could mediate antitumor responses in a distant tumor when administrated to one tumor locally. B16F10 cells were inoculated both in the left and in the right back of mice on day 0 (Fig. 5A). Subsequently, the αCD40 (50 μg/injection) forms were injected p.t. beside only the left tumor on day 4. The p.t. injection of PlGF-$2_{123\text{-}144}$-αCD40 slowed the outgrowth of both the left (ipsilateral) and right (contralateral) tumors; unmodified αCD40 did so as well, but to a significantly lesser extent. These data indicate that local PlGF-$2_{123\text{-}144}$-αCD40 treatment near one tumor enhances a systemic antitumor

immunological activity capable of reducing tumor growth systemically.

To investigate if the anti-tumor effect of PlGF-$2_{123-144}$-αCD40 treatment is dependent on $CD103^+$ DCs or $CD8\alpha^+$ DCs, we have employed *Batf3* gene knockout mice. Batf3, a basic leucine zipper transcription factor, is essential for the development of cross-presenting DCs such as $CD103^+$ DCs and of $CD8\alpha^+$ DCs (36-38). In *Batf3*$^{-/-}$ mice, the absence of these cross-presenting DCs severely compromises the cross-priming of $CD8^+$ T cells (39). Four days after B16F10 cell inoculation in *Batf3*$^{-/-}$ mice, PlGF-$2_{123-144}$-αCD40 (10 μg/injection) was administered p.t., as we have treated wild-type C57BL6 mice in Fig. 3A. Contrary to wild-type mice, PlGF-$2_{123-144}$-αCD40 treatment did not slow B16F10 tumor growth in *Batf3*$^{-/-}$ mice (Fig. 5B). This data suggests that the $CD103^+$ DC- or $CD8\alpha^+$ DC-mediated cross-priming of $CD8^+$ T cells plays a crucial role in the anti-tumor effect of PlGF-$2_{123-144}$-αCD40 treatment in B16F10 melanoma model.

To investigate the synergistic action between PlGF-$2_{123-144}$-αCD40 and CPI, we then treated B16F10 melanoma with αCD40 and CPI in combination. P.t. injection of CPI (unmodified αPD-L1 and αCTLA-4) did not show a significant anti-tumor effect

in combination with unmodified αCD40, whereas CPI significantly suppressed tumor growth in combination with PlGF-$2_{123-144}$-αCD40 (Fig. 5C). These data show that CPI and PlGF-$2_{123-144}$-αCD40 synergistically show an antitumor effect, probably through $CD8^+$ T cells.

PlGF-$2_{123-144}$-αCD40 treatment slows the growth of β-catenin-expressing genetically engineered primary melanomas

Our data demonstrated that PlGF-$2_{123-144}$-αCD40 treatment induces $CD8^+$ T cell infiltration in the B16F10 tumor (Fig. 4). We hypothesized that PlGF-$2_{123-144}$-αCD40 treatment may show antitumor efficacy against tumors with reduced T cell infiltration which are thus unresponsive to CPI therapy, through converting T cell non-inflamed tumors into inflamed tumors. To test this, we have employed *Tyr:Cre-ER*$^+$*/LSL-Braf*^{V600E}*/Pten*$^{fl/fl}$ *βCat*^{STA} mice, which are genetically engineered with Cre-inducible expression of active *B-Raf* and biallelic deletion of *PTEN*, commonly altered molecular pathways in human melanoma, with inducible expression of stabilized β-catenin (28). β-catenin pathway expression has been shown to reduce

infiltration of $CD103^+$ DCs, resulting in few T cells within the tumor microenvironment and unresponsiveness to CPI therapy (28). After tumor induction via local application of 4-OH-tamoxifen, unmodified or PlGF-$2_{123-144}$-αCD40 was administered via p.t. injection. Notably, p.t. administration of unmodified αCD40 slowed the growth of this tumor (Fig. 6A). More importantly, p.t. administration of PlGF-$2_{123-144}$-αCD40 treatment slowed tumor growth compared to PBS- and unmodified αCD40-treated groups (Fig. 6A). PlGF-$2_{123-144}$-αCD40 treatment but not αCD40 treatment prolonged survival (Fig. 6B).

Because PlGF-$2_{123-144}$-αCD40 treatment increased the frequency of $CD8^+$ T cells within B16F10 melanoma (Fig. 4G) and $CD8^+$ T cells are indispensable for antitumor effect by PlGF-$2_{123-144}$-αCD40 treatment (Fig. 3A and 5B), we analyzed the number of T cells in the *Tyr:Cre-ER*$^+$*/LSL-Braf*^{V600E}*/Pten*$^{fl/fl}$ *βCat*^{STA} tumors (Fig. 6D). PlGF-$2_{123-144}$-αCD40 treatment statistically significantly increased the frequency of $CD8^+$ T cells within tumor microenvironment compared to PBS treatment and unmodified αCD40 treatment. These data demonstrate that PlGF-$2_{123-144}$-αCD40 treatment shows an antitumor effect even within a CPI-unresponsive tumor, more so

than with the unmodified αCD40, consistent with the elevation of activated T cells observed in the B16F10 model.

Discussion

αCD40 as a cancer immunotherapeutic is associated with adverse events that limit the dosages of αCD40 that can be safely used in the clinic (11,40). In this study, the incidence of such adverse events was reduced by PlGF-$2_{123-144}$ conjugation to αCD40 when it was administered p.t., similarly to our previous observation with PlGF-$2_{123-144}$-conjugated CPI antibodies (27). PlGF-$2_{123-144}$-αCD40, which remains localized near the tumor tissue injection site, should more closely maintain normal systemic immune homeostasis by avoiding influences on non-tumor antigen-specific T or B cells and reducing influences on myeloid cells resident in the liver (32). It is likely that the lower hepatotoxicity and systemic cytokine release observed after PlGF-$2_{123-144}$-αCD40 administration was due to this reduction in systemic exposure. Notably, PlGF-$2_{123-144}$ conjugation may even allow decreases in the administered dose, as tumor growth delay was shown at low local dosages, where unmodified αCD40 had

no effect. These data suggest the possibility of treating patients who have discontinued therapy because of such adverse events, as well as who are not amenable to systemic therapy.

Of particular interest to us was the observation that αCD40 treatment suppressed the growth of *Tyr:Cre-ER^{+}/LSL-Braf^{V600E}/Pten$^{fl/fl}$ βCat^{STA}* melanoma, a CPI therapy unresponsive tumor (28). There are considerable numbers of patients who do not respond to CPI therapy, mainly because of low T cell infiltration (22). In the clinic, 48% of non-T-cell-infiltrated melanomas reportedly show active β-catenin signaling (28). Development of a treatment strategy that shows efficacy in a corresponding genetically engineered mouse tumor model would suggest the possibility of benefit for these patients. Our data show that PlGF-2$_{123-144}$-αCD40 treatment induced T cell infiltration into the *Tyr:Cre-ER^{+}/LSL-Braf^{V600E}/Pten$^{fl/fl}$ βCat^{STA}* melanoma tumor microenvironment. Given our observations of statistically elevated CD8^{+} T cell numbers in tumors of PlGF-2$_{123-144}$-αCD40-treated animals, and given the lack of response to therapy in CD103^{+}/CD8α^{+} DC-negative *Batf3$^{-/-}$* mice, we conclude that induction of antigen-specific CD8^{+} T cell response through cross-presentation of tumor

antigen drives the anti-tumor response more efficiently with PlGF-$2_{123-144}$-αCD40 treatment than with unmodified αCD40 treatment.

Our localized therapy also suppressed growth of a tumor contralateral to the injection site, which is consistent with earlier observations of induction of systemic immunity (2,41-43), although here through local action. Our data suggests the feasibility of treating patients with PlGF-$2_{123-144}$-αCD40 by injecting one accessible tumor site in metastatic disease. With the low concentration of PlGF-$2_{123-144}$-αCD40 in the blood combined with the increase in activated $CD8^+$ T cells in the tumor and the increase in induced anti-tumor cell antibody levels in the blood, the mechanism of action in a distant tumor is likely due to effective tumor antigen-specific immune cell activation, through which cytotoxic T lymphocytes and anti-tumor cell antibodies are disseminated systemically, rather than by leakage of PlGF-$2_{123-144}$-αCD40 from one tumor to the other. Unmodified αCD40 distributed systemically via p.t. administration did not significantly suppress B16F10 tumor growth as much as PlGF-$2_{123-144}$-αCD40. Because PlGF-$2_{123-144}$-αCD40 treatment activated $CD11c^+$ DCs, macrophages and B cells in the td-LN, we suppose that effective activation of antitumor B cells and T cells

through p.t. injection of αCD40 led to suppressed tumor outgrowth in both ipsilateral and contralateral tumors.

Local cancer immunotherapy has been tested in the clinic for melanoma, colorectal cancer, and lymphoma, exhibiting equivalent or higher antitumor efficacy compared to systemic administration of therapeutics (2,17,41-45). In a mouse model of colon carcinoma and thymoma, local administration of αCD40 with slow-release formulations (e.g. microparticle polymer, liposome and montanide oil emulsion) has enabled the use of lower doses of antibody, while maintaining or enhancing antitumor efficacy (2,17,46). In our study, we have rather explored a molecular engineering approach to improve the antitumor effects of αCD40 even more, by PlGF-$2_{123-144}$ peptide conjugation, to thus employ the tumor stroma or the peri-tumoral stroma as a depot for antibody retention. We show favorable effects both on efficacy and safety when injected p.t. in multiple tumor models.

In conclusion, we found that local injection of an ECM-binding variant of αCD40 has higher antitumor activity compared to its unmodified form, when administered p.t. Conjugation of PlGF-$2_{123-144}$ provided injection-site tissue retention of

αCD40. A clear reduction in systemic side effects was demonstrated, associated with lower αCD40 concentrations in the systemic circulation, including reduced cytokine release syndrome and reduced hepatotoxicity. Peri-tumoral injection of PlGF-$2_{123-144}$-αCD40 alters the tumor microenvironment and significantly activates APCs (with $CD103^+$ and or $CD8a^+$ DCs being essential), resulting in delayed tumor growth and prolonged survival, in addition to synergy with CPI therapy. This localized therapy also suppressed growth of a distant tumor. Importantly, favorable efficacy in a CPI-resistant melanoma model was observed; PlGF-$2_{123-144}$-αCD40 treatment enhanced T cell tumor-infiltration into this otherwise non-T cell inflamed tumor. This simple approach of engineering ECM-binding character into αCD40 may hold potential for clinical translation of αCD40 for localized delivery as a cancer immunotherapeutic.

Acknowledgements

We thank the Human Tissue Resource Center of the University of Chicago for histology analysis. Also we thank I. van Mier, E. A. Watkins, K. Sasaki, K. Katsumata, Y. Wang, S. Gomes, and S. Spranger for experimental advice and helpful discussions.

Authors' contributions:

Conception and design: J. Ishihara, A. Ishihara, J.A. Hubbell

Development of methodology: J. Ishihara, A. Ishihara, L. Potin, P. Hosseinchi, K. Fukunaga, M. Damo

Acquisition of data (provided animals, acquired and managed patients, provided facilities, etc.): J. Ishihara, A. Ishihara, L. Potin, P. Hosseinchi, T.F. Gajewski

Analysis and interpretation of data (e.g. statistical analysis, biostatistics, computational analysis): J. Ishihara, A. Ishihara, M.A. Swartz, J.A. Hubbell

Writing, review, and/or revision of the manuscript: J. Ishihara, A. Ishihara, T.F. Gajewski, M.A. Swartz, J.A. Hubbell

Administrative, technical, or material support (i.e., reporting or organizing data, constructing databases): T.F. Gajewski., M.A. Swartz, J.A. Hubbell

Study supervision: J. Ishihara, J.A. Hubbell

References:

1. Vonderheide RH, Glennie MJ. Agonistic CD40 antibodies and cancer therapy. Clin Cancer Res **2013**;19:1035-43

2. Fransen MF, Sluijter M, Morreau H, Arens R, Melief CJ. Local activation of CD8 T cells and systemic tumor eradication without toxicity via slow release and local delivery of agonistic CD40 antibody. Clin Cancer Res **2011**;17:2270-80

3. White AL, Chan HC, Roghanian A, French RR, Mockridge CI, Tutt AL, *et al.* Interaction with FcγRIIB is critical for the agonistic activity of anti-CD40 monoclonal antibody. J Immunol **2011**;187:1754-63

4. Jackaman C, Cornwall S, Graham PT, Nelson DJ. CD40-activated B cells contribute to mesothelioma tumor regression. Immunol Cell Biol **2011**;89:255-67

5. Lum HD, Buhtoiarov IN, Schmidt BE, Berke G, Paulnock DM, Sondel PM, *et al.* In vivo CD40 ligation can induce T-cell-independent antitumor effects that involve macrophages. J Leukoc biology **2006**;79:1181-92

6. Rakhmilevich AL, Alderson KL, Sondel PM. T-cell-independent antitumor effects of CD40 ligation. Int Rev Immunol **2012**;31:267-78

7. Rakhmilevich AL, Buhtoiarov IN, Malkovsky M, Sondel PM. CD40 ligation in vivo can induce T cell independent antitumor effects even against immunogenic tumors. Cancer Immunol Immunother : CII **2008**;57:1151-60

8. Hassan SB, Sorensen JF, Olsen BN, Pedersen AE. Anti-CD40-mediated cancer immunotherapy: an update of recent and ongoing clinical trials. Immunopharmacol Immunotoxicol **2014**;36:96-104

9. Johnson P, Challis R, Chowdhury F, Gao Y, Harvey M, Geldart T, *et al.* Clinical and biological effects of an agonist anti-CD40 antibody: a Cancer Research UK phase I study. Clin Cancer Res **2015**;21:1321-8

10. Beatty GL, Chiorean EG, Fishman MP, Saboury B, Teitelbaum UR, Sun W, *et al.* CD40 agonists alter tumor stroma and show efficacy against pancreatic carcinoma in mice and humans. Science **2011**;331:1612-6

11. Vonderheide RH, Flaherty KT, Khalil M, Stumacher MS, Bajor DL, Hutnick NA, *et al.* Clinical activity and immune modulation in cancer patients treated with

CP-870,893, a novel CD40 agonist monoclonal antibody. J Clin Oncol **2007**;25:876-83

12. Gladue RP, Paradis T, Cole SH, Donovan C, Nelson R, Alpert R, *et al.* The CD40 agonist antibody CP-870,893 enhances dendritic cell and B-cell activity and promotes anti-tumor efficacy in SCID-hu mice. Cancer Immunol Immunother : CII **2011**;60:1009-17

13. Kikuchi T, Moore MA, Crystal RG. Dendritic cells modified to express CD40 ligand elicit therapeutic immunity against preexisting murine tumors. Blood **2000**;96:91-9

14. Nimanong S, Ostroumov D, Wingerath J, Knocke S, Woller N, Gurlevik E, *et al.* CD40 signaling drives potent cellular immune responses in heterologous cancer vaccinations. Cancer Res **2017**;77:1918-26

15. Hojer C, Frankenberger S, Strobl LJ, Feicht S, Djermanovic K, Jagdhuber F, *et al.* B-cell expansion and lymphomagenesis induced by chronic CD40 signaling is strictly dependent on CD19. Cancer Res **2014**;74:4318-28

16. Mangsbo SM, Broos S, Fletcher E, Veitonmaki N, Furebring C, Dahlen E, *et al.*

The human agonistic CD40 antibody ADC-1013 eradicates bladder tumors and generates T-cell-dependent tumor immunity. Clin Cancer Res **2015**;21:1115-26

17. Rahimian S, Fransen MF, Kleinovink JW, Amidi M, Ossendorp F, Hennink WE. Polymeric microparticles for sustained and local delivery of antiCD40 and antiCTLA-4 in immunotherapy of cancer. Biomaterials **2015**;61:33-40

18. Sandin LC, Orlova A, Gustafsson E, Ellmark P, Tolmachev V, Totterman TH, *et al*. Locally delivered CD40 agonist antibody accumulates in secondary lymphoid organs and eradicates experimental disseminated bladder cancer. Cancer Immunol Res **2014**;2:80-90

19. 32nd annual meeting and pre-conference programs of the Society for Immunotherapy of Cancer (SITC 2017): part one National Harbor, MD, USA. 8-12 November 2017 Abstracts. J Immunother Cancer **2017**;5:86

20. Allison JP. Immune checkpoint blockade in cancer therapy: The 2015 Lasker-DeBakey clinical medical research award. JAMA **2015**;314:1113-4

21. Sharma P, Allison JP. The future of immune checkpoint therapy. Science **2015**;348:56-61

22. Topalian SL, Drake CG, Pardoll DM. Immune checkpoint blockade: a common denominator approach to cancer therapy. Cancer Cell **2015**;27:450-61

23. Patel SP, Kurzrock R. PD-L1 expression as a predictive biomarker in cancer immunotherapy. Mol Cancer Ther **2015**;14:847-56

24. Wang X, Teng F, Kong L, Yu J. PD-L1 expression in human cancers and its association with clinical outcomes. Onco Targets Ther **2016**;9:5023-39

25. Larkin J, Chiarion-Sileni V, Gonzalez R, Grob JJ, Cowey CL, Lao CD, *et al.* Combined nivolumab and ipilimumab or monotherapy in untreated melanoma. N Engl J Med **2015**;2015:23-34

26. Martino MM, Briquez PS, Guc E, Tortelli F, Kilarski WW, Metzger S, *et al.* Growth factors engineered for super-affinity to the extracellular matrix enhance tissue healing. Science **2014**;343:885-8

27. Ishihara J, Fukunaga K, Ishihara A, Larsson HM, Potin L, Hosseinchi P, *et al.* Matrix-binding checkpoint immunotherapies enhance antitumor efficacy and reduce adverse events. Sci Transl Med **2017**;9

28. Spranger S, Bao R, Gajewski TF. Melanoma-intrinsic beta-catenin signalling

prevents anti-tumour immunity. Nature **2015**;523:231-5

29. Liu W, Hou Y, Chen H, Wei H, Lin W, Li J, *et al.* Sample preparation method for isolation of single-cell types from mouse liver for proteomic studies. Proteomics **2011**;11:3556-64

30. Broggi MA, Schmaler M, Lagarde N, Rossi SW. Isolation of murine lymph node stromal cells. JoVE **2014**:e51803

31. Richman LP, Vonderheide RH. Role of crosslinking for agonistic CD40 monoclonal antibodies as immune therapy of cancer. Cancer Immunol Res **2014**;2:19-26

32. Byrne KT, Leisenring NH, Bajor DL, Vonderheide RH. CSF-1R-Dependent Lethal Hepatotoxicity When Agonistic CD40 Antibody Is Given before but Not after Chemotherapy. J Immunol **2016**;197:179-87

33. Ruter J, Antonia SJ, Burris HA, Huhn RD, Vonderheide RH. Immune modulation with weekly dosing of an agonist CD40 antibody in a phase I study of patients with advanced solid tumors. Cancer Biol Ther **2010**;10:983-93

34. Guy CT, Cardiff RD, Muller WJ. Induction of mammary tumors by expression

of polyomavirus middle T oncogene: a transgenic mouse model for metastatic disease. Mol Cell Biol **1992**;12:954-61

35. Ngiow SF, Young A, Blake SJ, Hill GR, Yagita H, Teng MW, *et al.* Agonistic CD40 mAb-driven IL12 reverses resistance to anti-PD1 in a T-cell-rich tumor. Cancer Res **2016**;76:6266-77

36. Martinez-Lopez M, Iborra S, Conde-Garrosa R, Sancho D. Batf3-dependent CD103+ dendritic cells are major producers of IL-12 that drive local Th1 immunity against Leishmania major infection in mice. Eur J Immunol **2015**;45:119-29

37. Edelson BT, Kc W, Juang R, Kohyama M, Benoit LA, Klekotka PA, *et al.* Peripheral CD103+ dendritic cells form a unified subset developmentally related to CD8alpha+ conventional dendritic cells. J Exp Med **2010**;207:823-36

38. Hildner K, Edelson BT, Purtha WE, Diamond M, Matsushita H, Kohyama M, *et al.* Batf3 deficiency reveals a critical role for CD8alpha+ dendritic cells in cytotoxic T cell immunity. Science **2008**;322:1097-100

39. Patel R, Sad S. Transcription factor Batf3 is important for development of CD8+

T-cell response against a phagosomal bacterium regardless of the location of antigen. Immunol Cell Biol **2016**;94:378-87

40. Vonderheide RH, Bajor DL, Winograd R, Evans RA, Bayne LJ, Beatty GL. CD40 immunotherapy for pancreatic cancer. Cancer Immunol Immunother : CII **2013**;62:949-54

41. Fransen MF, van der Sluis TC, Ossendorp F, Arens R, Melief CJ. Controlled local delivery of CTLA-4 blocking antibody induces CD8+ T-cell-dependent tumor eradication and decreases risk of toxic side effects. Clin Cancer Res **2013**;19:5381-9

42. Steiner M, Neri D. Antibody-radionuclide conjugates for cancer therapy: historical considerations and new trends. Clin Cancer Res **2011**;17:6406-16

43. Ellmark P, Mangsbo SM, Furebring C, Norlen P, Totterman TH. Tumor-directed immunotherapy can generate tumor-specific T cell responses through localized co-stimulation. Cancer Immunol Immunother : CII **2017**;66:1-7

44. Fransen MF, Ossendorp F, Arens R, Melief CJ. Local immunomodulation for cancer therapy: Providing treatment where needed. Oncoimmunology

2013;2:e26493

45. Marabelle A, Kohrt H, Caux C, Levy R. Intratumoral immunization: a new paradigm for cancer therapy. Clin Cancer Res **2014**;20:1747-56

46. Kwong B, Liu H, Irvine DJ. Induction of potent anti-tumor responses while eliminating systemic side effects via liposome-anchored combinatorial immunotherapy. Biomaterials **2011**;32:5134-47

Figure Legends

Fig. 1. PlGF-$2_{123-144}$ conjugated αCD40 binds to ECM proteins and shows prolonged injection-site tissue retention.

A, PlGF-$2_{123-144}$- and unmodified αCD40 were analyzed by SDS-PAGE under reducing conditions with coomassie blue staining. B, PlGF-$2_{123-144}$- and unmodified αCD40 binding affinities to fibronectin, vitronectin and collagen I were measured by ELISA. A450 nm represents absorbance at 450 nm. BSA served as a negative control (n = 6, mean ± SD). C, PlGF-$2_{123-144}$- and unmodified αCD40 binding affinities to recombinant mouse CD40 was measured by ELISA. A450 nm represents absorbance at 450 nm (n = 4, mean ± SD). D, Skin tissue retention of PlGF-$2_{123-144}$-αCD40 was tested in the *in vivo* imaging system. Cyanine 7-labeled PlGF-$2_{123-144}$- and unmodified αCD40 were injected in the back skin of athymic nude mice, followed by imaging every 24 hr. The graph represents a time profile of quantification of signal intensity by performing a region-of-interest (ROI) analysis. Fluorescence intensity by measuring the ROI was normalized by initial fluorescence intensity (n = 5, mean ± SEM). Two experimental replicates. Statistical analyses were done using a two-tailed Student's *t*-test. $^{**}p < 0.01$.

Fig. 2. PlGF-$2_{123-144}$ conjugation reduces systemic exposure to αCD40 and treatment-related toxicity.

5×10^5 B16F10 cells were inoculated on day 0. PlGF-$2_{123-144}$-αCD40 (50 μg), αCD40, or PBS was administered on day 4 p.t. A, Blood serum was collected on day 4 (4 hr after injection), 6, and 8. The concentration of αCD40 in blood serum was determined by ELISA (n = 6, mean ± SEM). B-C, Concentrations of IL-6 and TNFα in blood serum were measured by ELISA (n = 6, mean ± SEM). D, ALT levels in serum were measured (n = 9-14, mean ± SEM). E, Histologic liver sections 3 days after p.t. injection of 50 μg PlGF-$2_{123-144}$-αCD40, αCD40, or PBS. Scale bar = 400 μm. Representative sections of groups of 3 mice. Statistical analyses were done using ANOVA with Tukey's test using the values of each day. Two experimental replicates. $*p < 0.05$; $**p < 0.01$; N.S. = not significant.

Fig. 3. PlGF-$2_{123-144}$-αCD40 suppresses growth of multiple tumors compared to unmodified αCD40.

A-B, 5×10^5 B16F10 melanoma cells were inoculated in the back skin on day 0. A, 10 μg or B, 50 μg of PlGF-$2_{123\text{-}144}$-αCD40, αCD40, or PBS was administered on day 4 (A; n = 8-9, B; n = 8-9). C, 5×10^5 CT26 colon carcinoma cells were inoculated in the back skin on day 0. 10 μg of PlGF-$2_{123\text{-}144}$-αCD40, αCD40, or PBS was administered on day 5 (n = 6-7). D, 8×10^5 MMTV-PyMT breast cancer cells were inoculated into the right mammary fat pad. 50 μg of PlGF-$2_{123\text{-}144}$-αCD40, αCD40, or PBS was administered on day 7 (n = 7-9). Antibody was injected p.t. The graph depicts tumor volume until the first mouse in each group died. Tumor volumes are presented as mean ± SEM. Statistical analyses were done using ANOVA with Tukey's test or Student's t-test. $**p < 0.01$, $*p < 0.05$.

Fig. 4. PlGF-$2_{123\text{-}144}$-αCD40 treatment activates T cells, B cells, DCs, and macrophages within tumor.

5×10^5 B16F10 cells were inoculated on day 0. 50 μg of PlGF-$2_{123\text{-}144}$-αCD40, αCD40, or PBS was administered on day 4. αCD40 was injected p.t. A-L, Tumor and td-LN were taken on day 9, followed by flow cytometric analysis. Graphs depict the % of A,

$CD11c^+$ DCs of $CD45^+$ lymphocytes within tumor. B, $CD11c^+$ DCs of $CD45^+$ lymphocytes within td-LN. C, $MHCII^{High}CD86^+$ cells of $CD11c^+$ DCs within tumor. D, $MHCII^{High}CD86^+$ cells of $CD11c^+$ DCs within td-LN. E, $MHCII^{High}CD86^+$ cells of $F4/80^+$ macrophages within tumor. F, $MHCII^{High}CD86^+$ cells of $F4/80^+$ macrophages within td-LN. G, $CD8^+CD3^+$ T cells of $CD45^+$ lymphocytes within tumor. H, $CD62L^-CD44^+$ effector cells of $CD8^+CD3^+$ T cells within tumor. I, $CD4^+CD3^+$ T cells of $CD45^+$ lymphocytes within tumor. J, $CD25^+Foxp3^+$ Treg cells of $CD4^+CD3^+$ T cells within tumor. K, The cell number ratio of $CD62L^-CD44^+CD8^+CD3^+$ effector T cells / $CD25^+Foxp3^+CD4^+CD3^+$ Treg cells within tumor. L, $PD\text{-}1^+$ cells of $CD8^+CD3^+$ T cells within tumor. M-O, Tumor, td-LN, and blood plasma were taken on day 11. M, $MHCII^{High}CD86^+$ cells of $B220^+$ B cells within tumor. N, $MHCII^{High}CD86^+$ cells of $B220^+$ B cells within td-LN. O, Mean fluorescence intensity by flow cytometry of endogenous anti-B16F10 cells antibodies. Bars represent mean ± SEM. Two experimental replicates. Statistical analyses were done using ANOVA with Tukey's test. $*p < 0.05$; $**p < 0.01$.

Fig. 5. PlGF-$2_{123-144}$-αCD40 treatment induces systemic antitumor immunity.

A, 5×10^5 B16F10 cells were inoculated intradermally on day 0 both in the left and right sides of mouse back skin. 50 μg of PlGF-$2_{123-144}$-αCD40, αCD40 or PBS was administered on day 4. P.t. injections were performed only beside the left tumor, but not the right tumor. Tumor volumes of the tumor on the left back and the tumor on the right back were measured (n = 9, mean ± SEM). B, 5×10^5 B16F10 melanoma cells were inoculated in the back skin of *Batf3*$^{-/-}$ mice on day 0. 10 μg of PlGF-$2_{123-144}$-αCD40 or PBS was administered on day 4. Tumor volumes are presented as mean ± SEM (n = 9). C, 5×10^5 B16F10 cells were inoculated intradermally on day 0 in the mouse back skin. 10 μg of PlGF-$2_{123-144}$-αCD40 or αCD40 and CPI (αPD-L1 and αCTLA4, 100 μg each, unmodified) were administered p.t. on day 5. Tumor volumes of the tumor were measured (n = 8-10, mean ± SEM). Two experimental replicates. Statistical analyses were done using ANOVA with Tukey's test or Student's t-test. *$p < 0.05$; **$p < 0.01$; N.S. = not significant.

Fig. 6. PlGF-$2_{123-144}$-αCD40 treatment shows antitumor activity against

β-catenin-expressing genetically engineered primary melanomas.

Tyr:Cre-ER^{+}*/LSL-Braf*^{V600E}*/Pten*$^{fl/fl}$ *βCat*^{STA} mice received 50 μg of 4-OH-tamoxifen on their back skin to induce melanoma development. Day 0 is defined as the time point when tumors first become visible. PlGF-$2_{123-144}$-αCD40, αCD40, or PBS was injected p.t. on days 0 and 7. αCD40 was injected at 10 μg of each/injection. A, Tumor sizes are shown (n = 6, mean ± SEM). B, Survival rates are shown (n = 6). C, The density of $CD8^{+}CD3^{+}$ T cells in the *Tyr:Cre-ER*$^{+}$*/LSL-Braf*^{V600E}*/Pten*$^{fl/fl}$ *βCat*^{STA} tumor is shown (mean ± SEM). 3-4 fields of images per tumor were taken, and the average T cell density was calculated. Two experimental replicates. Statistical analyses were done using ANOVA with Tukey's test. For single comparisons, a two-tailed Student's *t*-test was used. Log-rank (Mantel-Cox) test for survival curves. *$p < 0.05$; **$p < 0.01$.

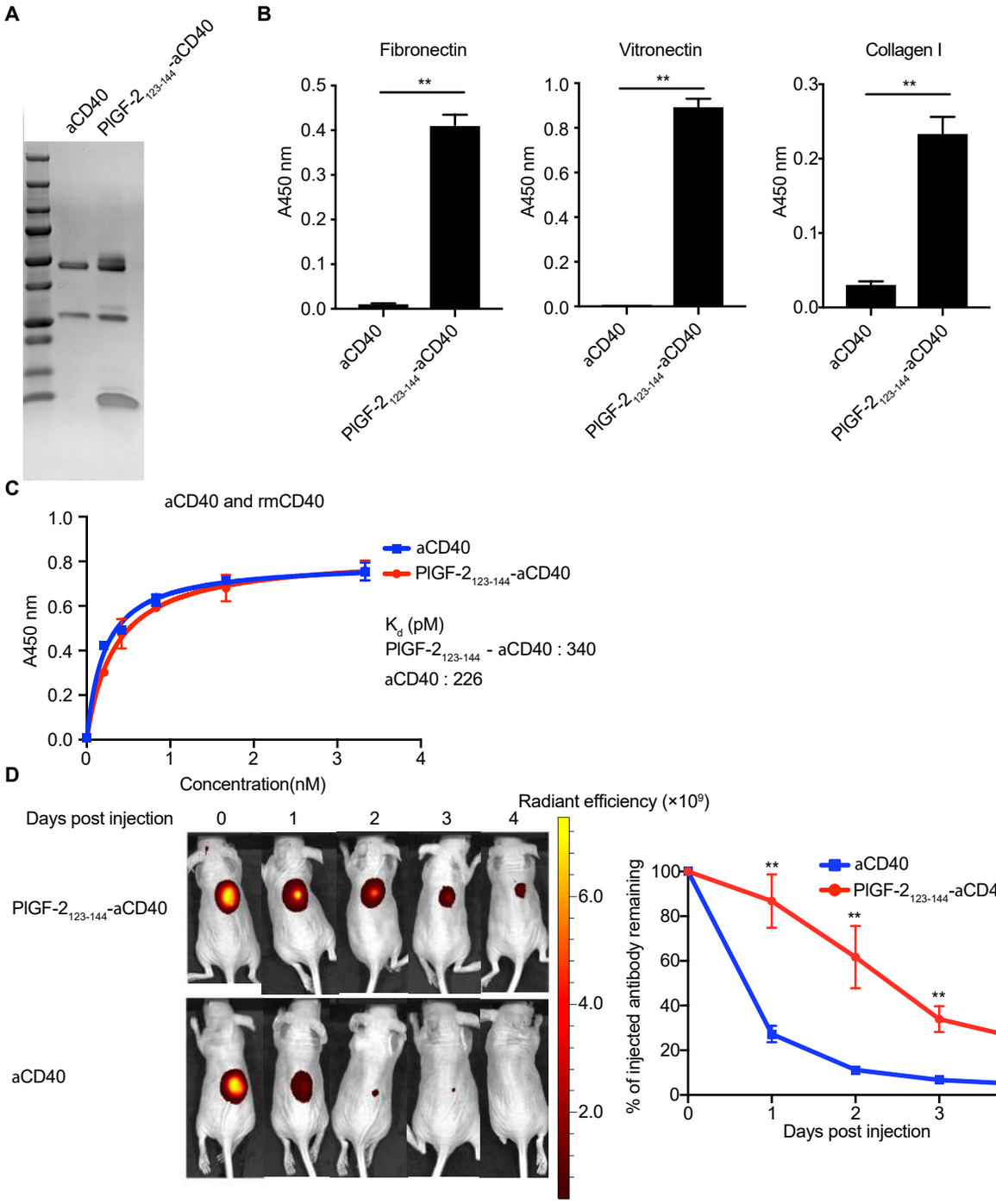
A
aCD40
PlGF-2123-144-aCD40
B
Fibronectin
Vitronectin
Collagen I
A450 nm
**
aCD40
PlGF-2123-144-aCD40
C
aCD40 and rmCD40
A450 nm
Concentration(nM)
aCD40
PlGF-2123-144-aCD40
Kd (pM)
PlGF-2123-144 - aCD40 : 340
aCD40 : 226
D
Days post injection
0
1
2
3
4
PlGF-2123-144-aCD40
aCD40
Radiant efficiency (×10⁹)
6.0
4.0
2.0
% of injected antibody remaining
Days post injection

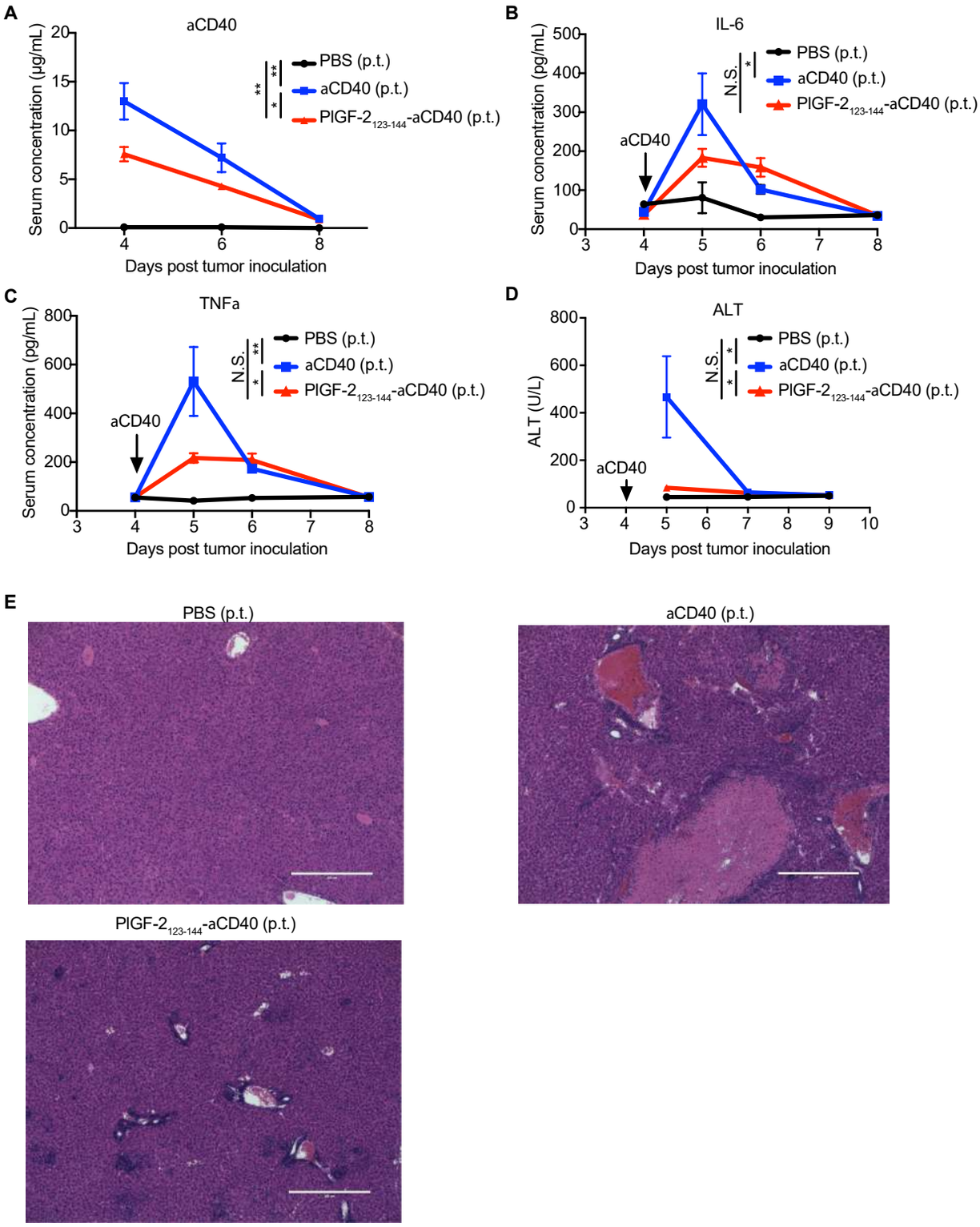
A
aCD40
Serum concentration (μg/mL)
Days post tumor inoculation
PBS (p.t.)
aCD40 (p.t.)
PlGF-2123-144-aCD40 (p.t.)
B
IL-6
Serum concentration (pg/mL)
N.S.
aCD40
C
TNFa
D
ALT
ALT (U/L)
E
PBS (p.t.)
aCD40 (p.t.)
PlGF-2123-144-aCD40 (p.t.)

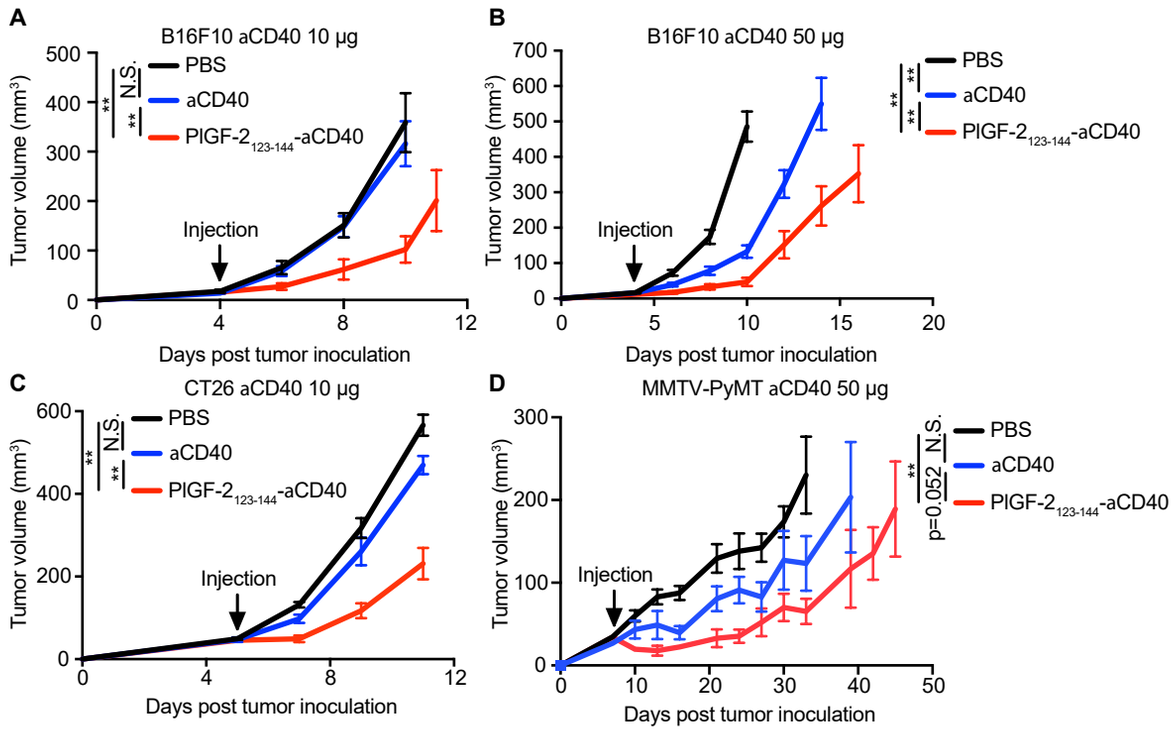
A
B16F10 aCD40 10 μg
Tumor volume (mm3)
Days post tumor inoculation
Injection
PBS
aCD40
PlGF-2123-144-aCD40
N.S.
**
**
B
B16F10 aCD40 50 μg
C
CT26 aCD40 10 μg
D
MMTV-PyMT aCD40 50 μg
p=0.052

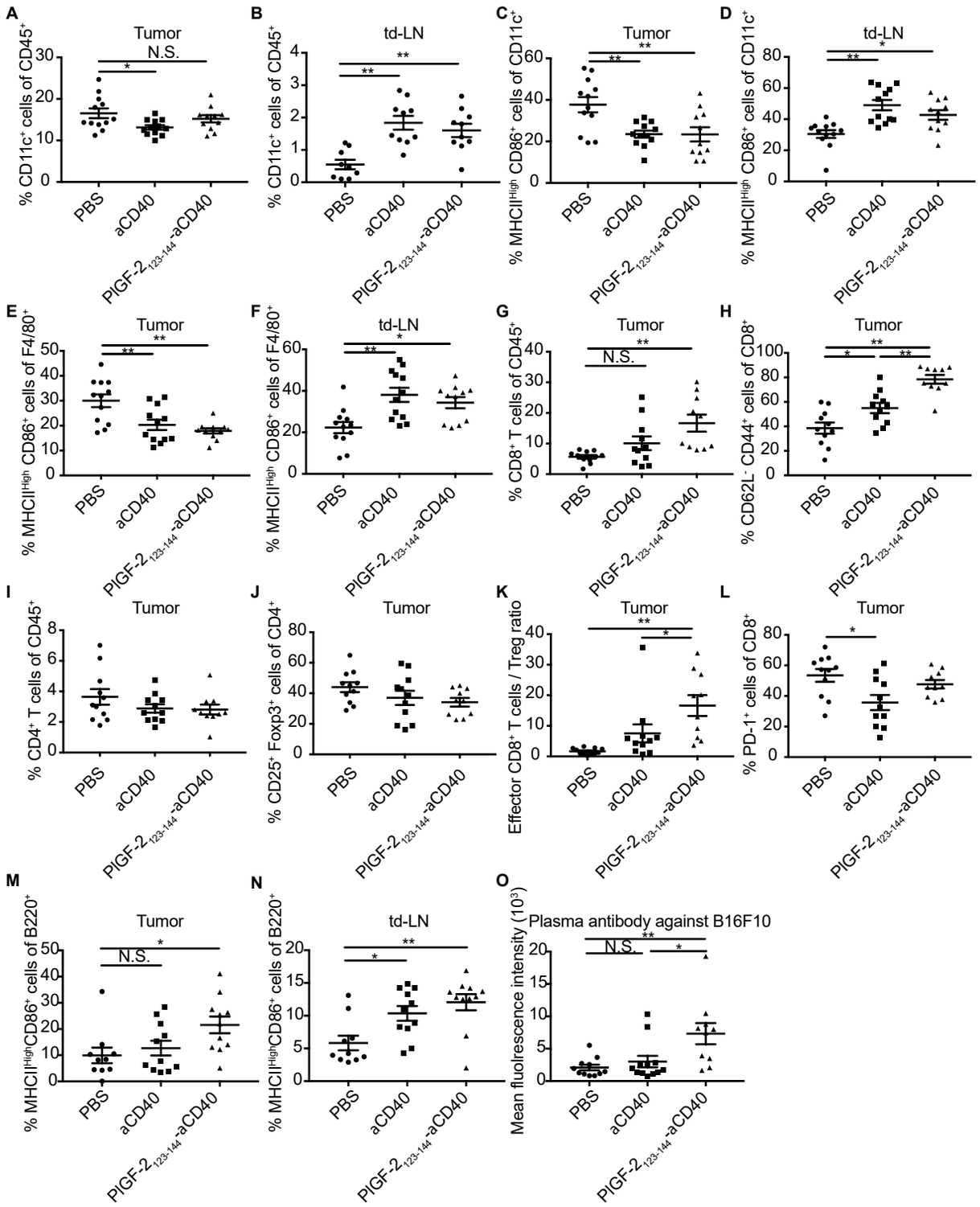
A
Tumor
N.S.
% CD11c+ cells of CD45+
B
td-LN
% CD11c+ cells of CD45+
C
Tumor
% MHCIIHigh CD86+ cells of CD11c+
D
td-LN
% MHCIIHigh CD86+ cells of CD11c+
E
Tumor
% MHCIIHigh CD86+ cells of F4/80+
F
td-LN
% MHCIIHigh CD86+ cells of F4/80+
G
Tumor
N.S.
% CD8+ T cells of CD45+
H
Tumor
% CD62L- CD44+ cells of CD8+
I
Tumor
% CD4+ T cells of CD45+
J
Tumor
% CD25+ Foxp3+ cells of CD4+
K
Tumor
Effector CD8+ T cells / Treg ratio
L
Tumor
% PD-1+ cells of CD8+
M
Tumor
N.S.
% MHCIIHighCD86+ cells of B220+
N
td-LN
% MHCIIHighCD86+ cells of B220+
O
Plasma antibody against B16F10
N.S.
Mean fluolrescence intensity (10³)
PBS
aCD40
PIGF-2123-144-aCD40

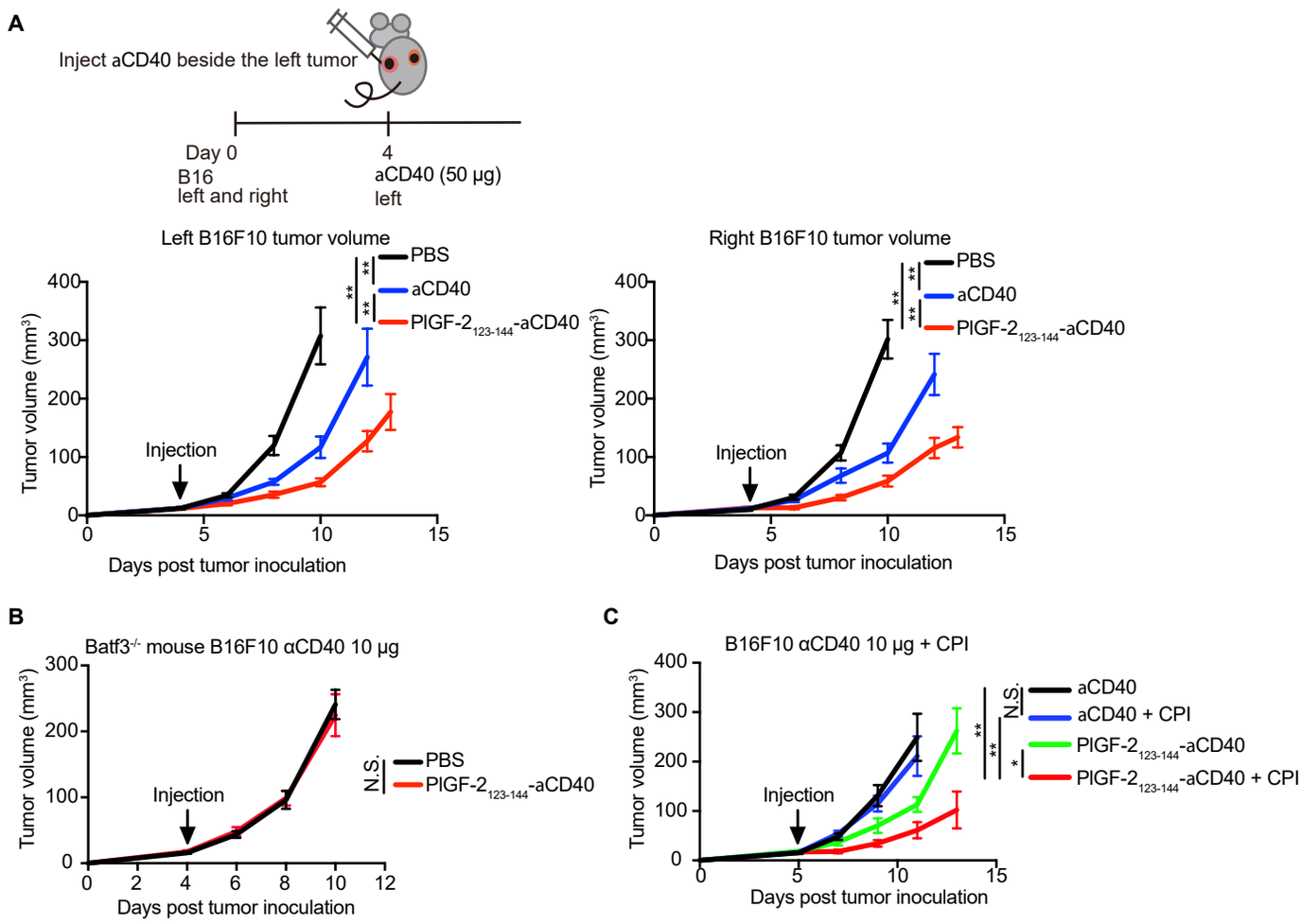
A
Inject aCD40 beside the left tumor
Day 0
B16
left and right
4
aCD40 (50 μg)
left
Left B16F10 tumor volume
Right B16F10 tumor volume
PBS
aCD40
PIGF-2123-144-aCD40
Tumor volume (mm3)
Injection
Days post tumor inoculation
**
B
Batf3-/- mouse B16F10 αCD40 10 μg
N.S.
C
B16F10 αCD40 10 μg + CPI
aCD40 + CPI
PIGF-2123-144-aCD40 + CPI
*

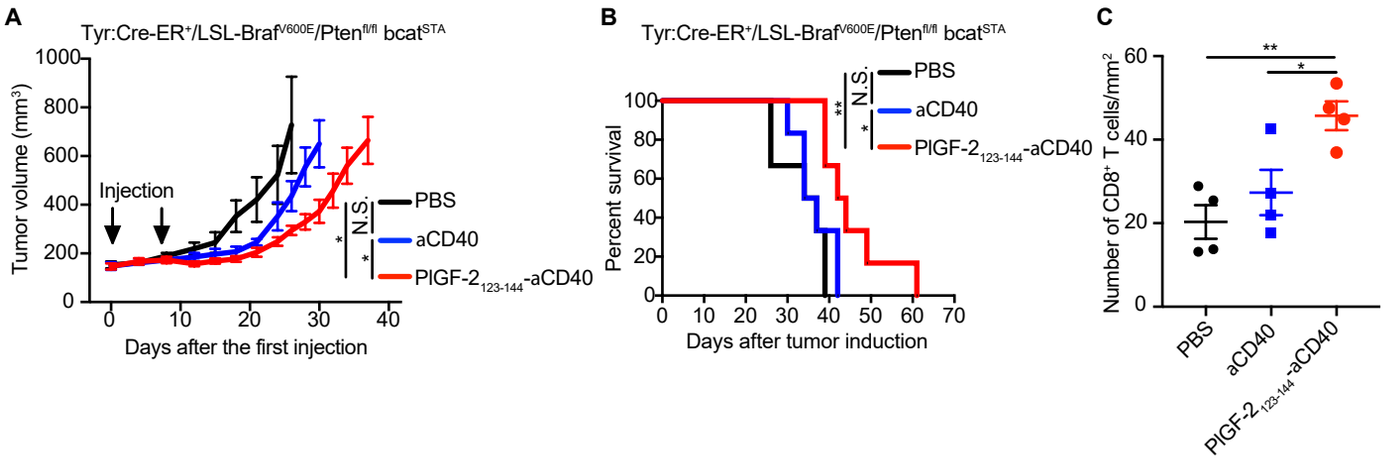
A
Tyr:Cre-ER+/LSL-Braf V600E/Pten fl/fl bcat STA
Tumor volume (mm3)
1000
800
600
400
200
0
Injection
0
10
20
30
40
Days after the first injection
N.S.
*
*
PBS
aCD40
PIGF-2123-144-aCD40
B
Tyr:Cre-ER+/LSL-Braf V600E/Pten fl/fl bcat STA
Percent survival
100
80
60
40
20
0
0
10
20
30
40
50
60
70
Days after tumor induction
**
N.S.
*
PBS
aCD40
PIGF-2123-144-aCD40
C
Number of CD8+ T cells/mm2
60
40
20
0
**
*
PBS
aCD40
PIGF-2123-144-aCD40